Pure Appl. Geophys. 177 (2020), 497–508

https://doi.org/10.1007/s00024-019-02286-1

Pure and Applied Geophysics

Using a Structure Correction Method to Improve the Location Accuracy of the Hotan Seismic Array

Chunyue Hao[1] and Li Li[1]

Abstract—A structure correction method is investigated and used to improve the location results of the Wenchuan, Pishan, and 171 other earthquakes using the Hotan seismic array data. Systematic slowness anomalies are found between frequency–wavenumber analysis and the location results from the China Earthquake Network Center, and all slowness error vectors point to about 300°. It is found that the back-azimuth and slowness errors change from positive to negative as the back-azimuth of different ray paths turns from north to south and from east to west, respectively. This phenomenon can be attributed to a dipping layer beneath the array with strike, dip, and velocity contrast of 210°, 45°, and 0.78, respectively. After correction for this dipping structure, the location results of the two main sequences are improved by 25.5% and 70.8% in terms of back-azimuth and slowness, respectively. Moreover, the location results of the other 171 earthquakes are improved by 28.5% and 7.1% in terms of back-azimuth and slowness, respectively.

Key words: Hotan array, systematic error, dipping layer, location improvement.

1. Introduction

Small-aperture seismic arrays are installed to detect weak seismic signals. In the 1960s, many seismic arrays were built by British and American researchers, and scientists used the array data to develop specific methods for data processing because the waveforms from a particular array appear similar. The basic method used to locate an earthquake based on a small-aperture seismic array is frequency–wavenumber (F–K) analysis. This method can indicate the back-azimuth and slowness; however, large systematic errors are sometimes found when applying F–K analysis to array data. Some studies have attributed such systematic errors to lateral velocity variations in the deep mantle (Weichert 1972; Davies and Sheppard 1972; Kanasewich et al. 1972, 1973; Sengupta and Julian 1974; Powell 1975). Conversely, others have attributed the observed anomalies to lateral velocity variations in the crust and upper mantle (Hearty et al. 1977; Briden et al. 1982; Walck and Minster 1982; Granet 1986; Dainty and Battis 1989). Other research has indicated that such large systematic errors are due to crustal effects beneath recording sites (Niazi and Anderson 1965; Niazi 1966; Sheppard 1967; Chinnery and Toksoz 1967; Cleary et al. 1968; Greenfield and Sheppard 1969; Wright et al. 1974; Lin and Roecker 1996). During such studies, researchers have noted a strange phenomenon regarding the distribution of location vectors, viz. that the location vectors in a slowness diagram point in a single direction for some arrays. After investigation, it was found that this phenomenon is related to a dipping layer below the array. Structural corrections should thus be applied to seismic array data to obtain satisfactory location results when such structure-related systematic errors are found. Previous studies have introduced one or several dipping interfaces to perform structure correction for arrays (Berteussen et al. 1977; Ram and Yadav 1984; Lin and Roecker 1996) to compensate the systematic errors generated during the location process.

A similar phenomenon of slowness has been found at the Hotan array. The Hotan seismic array is located at the northwest margin of the Tibetan Plateau and the southwest margin of the Tarim Basin. Multigroup reflections inclining to the north under the West Kunlun Mountains and to the south under the Tarim Basin have been observed using a deep seismic

[1] Institute of Geophysics, China Earthquake Administration, No.5 Minzudaxue South Road, Haidian District, Beijing 100081, China. E-mail: haovanilla@sina.com; lilygrace@cea-igp.ac.cn

reflection profile, as evidence for the face-to-face tilted collision of the Tarim and northwestern Tibetan lithosphere under the West Kunlun Mountains (Gao et al. 2000). Kao et al. (2001) also reported the existence of both north- and south-dipping upper mantle structures under the Kunlun foreland and the Kunlun Shan region, respectively.

The aim of this study is to determine whether there is a dipping layer in the crust or a dipping Moho related with the location errors observed at the Hotan array.

2. Background of the Hotan Array

The Hotan array is installed in Pishan County in the Hotan region. The Kunlun Mountain is to its south, and the peak of the Piyaman anticline is at its east side. The surrounding area is hilly with a central flat valley. In this area, the bedrock is widely exposed.

The Hotan array comprises nine elements equipped with short-period three-component seismometers and distributed with a 3-km aperture arranged in two circles (Fig. 1a). The code of the central element is HTTZ1, and there is a three-component broadband seismometer installed in the vault beside one short-period seismometer. The back-azimuth monitoring capability of this array is satisfactory, and it meets the needs of this study (Fig. 1b). Compared with a medium-aperture seismic array, the main lobe of the small-aperture array is larger because of its aperture size. Its slowness resolution is low, and the maximum error should be 4 s/°, according to the results of Koch and Kradolfer (1999). The standard error for the back-azimuth is about 20°. The side lobes that appear in the array response are the result of the large distances between the elements.

3. Analysis of Earthquakes Recorded by the Hotan Small-Aperture Seismic Array

According to Otsuka (1966), the location of a slowness anomaly can be determined using special datasets. In this study, the slowness anomaly of the Hotan array is analyzed using three datasets: the Pishan earthquakes (local, epicenter distances $\sim 0.8°$), Wenchuan earthquakes (regional, epicenter distances $\sim 21°$), and 171 other earthquakes with different directions (most being teleseismic events with epicenter distances $> 30°$). The similar ray paths of the earthquake sequences should eliminate errors associated with crustal inhomogeneity.

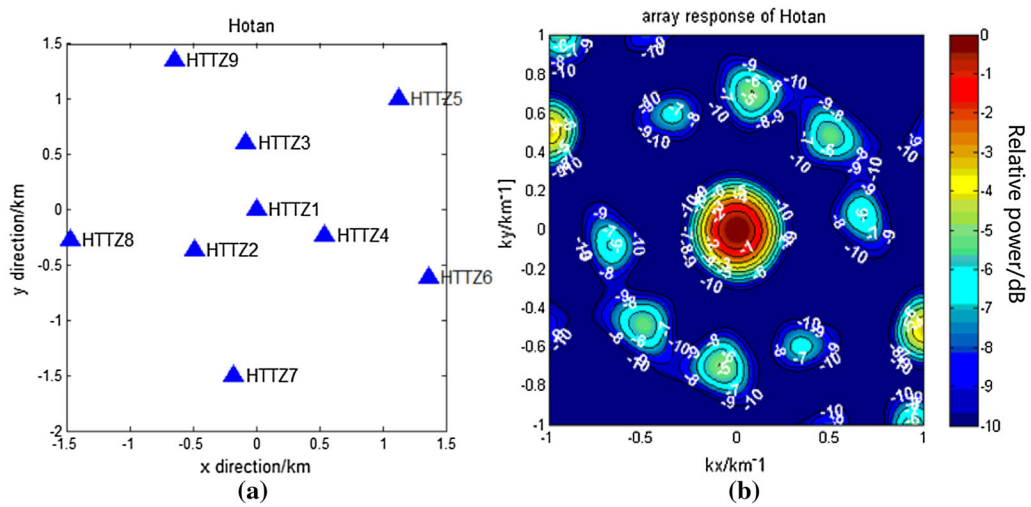

Figure 1
Distribution of Hotan array sites and array response function: **a** elements deployed in the Hotan array and **b** Hotan array response. The isoline interval is 1 dB

Moreover, large-magnitude earthquakes are selected to provide higher signal-to-noise ratio (SNR) to avoid misreading errors.

When locating an earthquake using seismic array data, several factors can affect the calculation of the azimuth and the slowness errors, one of which is the assumption of a plane wavefront with constant velocity. For $\Delta < 20°$, the effect of wavefront curvature becomes significant. The change in apparent wave slowness given by $dT/d\Delta$ with the change in epicentral distance is another source of error. According to the tables of Jeffreys–Bullen, $dT/d\Delta$ changes by < 0.2 s/° for a difference in epicentral distance of 2° when $\Delta > 30°$. For $\Delta < 30°$, and especially for $\Delta < 20°$, the change in $dT/d\Delta$ is irregular; For example, sometimes a change of 2° in epicentral distance might be associated with a change in $dT/d\Delta$ of > 1 s/°, while a change of 3° in epicentral distance might result in no change in $dT/d\Delta$. Ideally, the shortest epicentral distances used without correction in this type of analysis should be at least 30° (Otuska 1966).

Otuska (1966) stated that, if locations are affected by a structure, all events should be corrected to eliminate the effect of that structure. Generally, if the slowness error vectors appear random, it is appropriate to use the slowness–azimuth station correction method. However, if the slowness error vectors appear to have systematic errors, such errors should be analyzed and eliminated first. Then, when the systematic characteristics have been removed from the errors, the slowness–azimuth station correction method should be used for the remaining random errors.

In this study, the final research results could not be affected by the structure-related systematic errors, because the manuscript mainly studied the cause and source of these errors, so the entire research process did not include error accumulation. A dipping layer model is built to compensate these errors. The parameters of the model and the source location are the final research results.

For local events, errors contain large components of uncertainty and irregularity relative to teleseismic events. Therefore, the location results of local events can be improved obviously through correction by taking the catalog from the local network as reference values.

3.1. F–K Analysis for Pishan Earthquake

On July 3, 2015, the Hotan array recorded the Pishan earthquake (Fig. 2). According to the catalog from the Chinese Earthquake Networks Center (CENC), the latitude, longitude, and depth of the earthquake were 37.6°N, 78.2°E, and 10 km, respectively, corresponding to 302.70°, 14.03 s/°, and 96 km in terms of back-azimuth, slowness, and distance from the Hotan array.

F–K analysis can calculate the back-azimuth and horizontal slowness simultaneously (Capon 1973; Harjes and Henger 1973; Aki and Richards 1980). The time differences between the elements of the array can be used to estimate the slowness vector. If the back-azimuth and slowness are unknown, the combination of the two parameters will be searched to find the largest accumulation values for all of the elements. To save time, the calculations are carried out in the frequency domain. Thus, the Pishan earthquake is analyzed and the back-azimuth and slowness determined to be 298.30° and 7.09 s/°, respectively (Fig. 3). The results from the CENC are taken as the theoretical values, while the F–K analysis results are considered to be the observed values. Thus, it is determined that the errors of the back-azimuth and slowness are −4.4° and −6.94 s/°, respectively. The back-azimuth error value is normal, whereas the slowness error is too large.

3.2. Location Vectors of Pishan Sequence

To investigate the reason for the large slowness error, 83 events from the Pishan earthquake sequence that occurred during July 3–15, 2015 are analyzed (Table 1). The catalog results from the CENC are taken as theoretical values, and the F–K analysis results are considered to be the observation values. Thus, the location errors of the Pishan events recorded by the Hotan array are obtained (Fig. 4a). In Fig. 4a, red circles represent observed values, blue dots represent theoretical location results, and red lines point to theoretical values. The center of the diagram represents the Hotan array. The back-

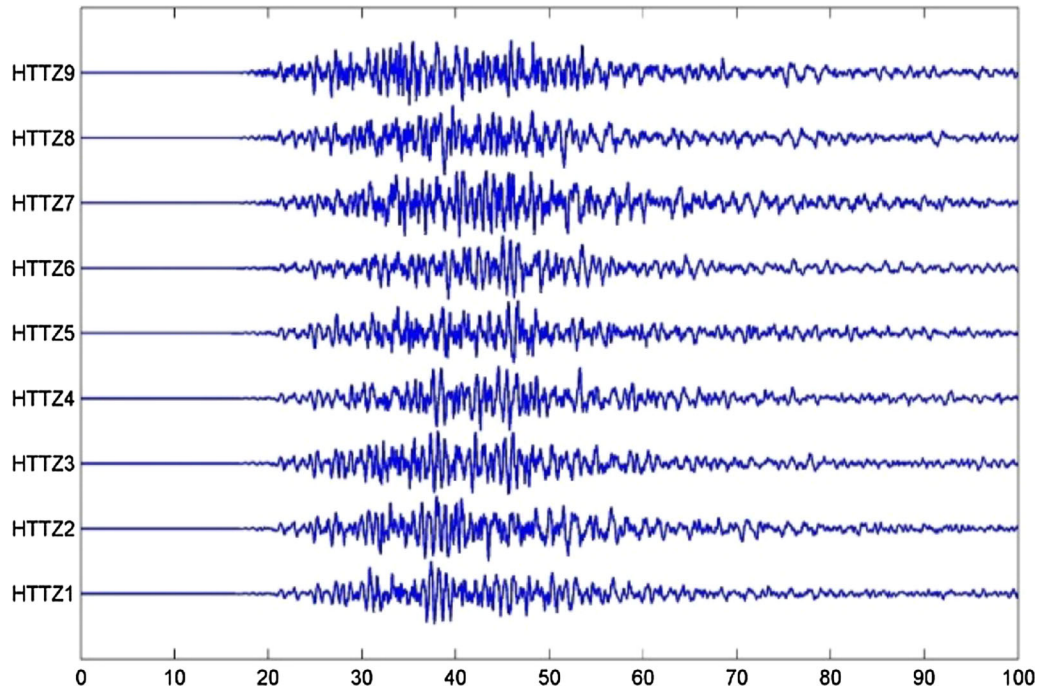

Figure 2
Waveforms of Pishan earthquake on July 3, 2015, as recorded by the Hotan array

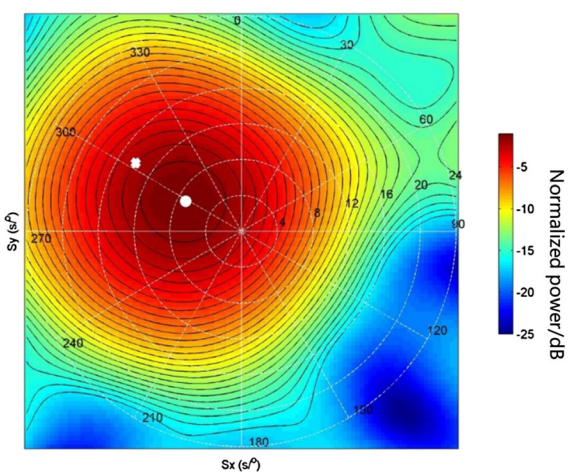

Figure 3
F–K analysis for Pishan earthquake on July 3, 2015; azimuth is read clockwise from north, while slowness is read in radial direction. The region inside the innermost contour represents the maximum energy, and the white dot represents the location of the maximum value; the parameters are 298.30°and 7.09 s/°, respectively. Similarly, the white cross represents the theoretical value from the CENC; the corresponding parameters are 302.70° and 14.03 s/°, respectively

azimuth can be read clockwise from north (one tick every 30°), while slowness values can be read radially (one tick every 4 s/°).

For a small-aperture seismic array with isotropic conditions and simple structure, the location vectors should be random. It can be seen from Fig. 4a that the back-azimuth errors are small while the slowness errors are large. The fact that the location vectors all point in one direction (at $\sim$ 300°) means that all the observation values are smaller than the theoretical values. This phenomenon indicates that the errors are not random but systematic.

Systematic errors in slowness are also called slowness anomalies. The main reasons for such systematic errors include geology, seismometers, human activity, and other factors. The seismometers were checked and the surroundings investigated to exclude these as possible sources of error. Thus, it is concluded that the reason for the systematic error shown in the Hotan array data is related to geological conditions below the array.

Table 1

Catalog of events in Pishan earthquake sequence with magnitude > 3.0

Date	Origin time	Latitude	Longitude	Depth	Magnitude	Place
2015/7/15	9:01:17	37.6	77.9	10	3.6	Pishan County
2015/7/15	3:27:29	37.5	78.2	10	3	Pishan County
2015/7/14	20:29:11	37.6	77.8	10	4	Pishan County
2015/7/14	16:38:48	37.5	78.1	10	3.3	Pishan County
2015/7/14	14:07:23	37.5	78	10	4.2	Pishan County
2015/7/12	17:12:07	37.6	78	10	3.3	Pishan County
2015/7/11	6:06:03	37.5	78.1	10	3.1	Pishan County
2015/7/10	5:19:17	37.5	78.1	9	3	Pishan County
2015/7/10	1:54:13	37.5	78.1	10	3.4	Pishan County
2015/7/9	18:03:52	37.5	78.1	10	3.1	Pishan County
2015/7/9	14:08:47	37.5	78.1	7	3.2	Pishan County
2015/7/9	13:48:54	37.5	78.1	10	3.1	Pishan County
2015/7/9	13:39:51	37.5	78.1	7	3.2	Pishan County
2015/7/8	22:06:39	37.5	78.1	10	3	Pishan County
2015/7/8	20:45:29	37.6	78.1	6	3.1	Pishan County
2015/7/7	21:51:31	37.6	78	10	3	Pishan County
2015/7/7	4:14:46	37.5	77.9	10	3.2	Pishan County
2015/7/7	3:35:09	37.5	78.1	10	3	Pishan County
2015/7/7	3:22:39	37.5	77.9	10	3.7	Pishan County
2015/7/6	20:58:17	37.6	77.9	10	3.3	Pishan County
2015/7/6	10:28:57	37.5	78.1	10	3	Pishan County
2015/7/6	9:32:33	37.5	78.2	10	3.1	Pishan County
2015/7/6	3:06:16	37.6	78	7	3.6	Pishan County
2015/7/5	23:12:11	37.5	78	9	3.6	Pishan County
2015/7/5	18:43:17	37.5	78.1	8	3	Pishan County
2015/7/5	8:35:29	37.6	78	10	3	Pishan County
2015/7/5	3:23:03	37.6	78	10	3	Pishan County
2015/7/5	2:18:41	37.6	77.9	10	3	Pishan County
2015/7/4	22:37:44	37.5	78.1	10	3.1	Pishan County
2015/7/4	22:26:14	37.5	78	10	3	Pishan County
2015/7/4	16:53:34	37.6	78.1	10	3	Pishan County
2015/7/4	15:07:23	37.5	78.1	10	3	Pishan County
2015/7/4	11:08:48	37.5	78.1	10	3.2	Pishan County
2015/7/4	10:49:44	37.5	78	10	3	Pishan County
2015/7/4	8:36:37	37.5	78	9	3.6	Pishan County
2015/7/4	8:13:10	37.5	77.9	10	3.2	Pishan County
2015/7/4	7:49:01	37.6	78.1	10	3.2	Pishan County
2015/7/4	6:32:47	37.5	78	10	3	Pishan County
2015/7/4	4:36:12	37.6	77.8	10	3	Pishan County
2015/7/4	4:00:41	37.5	78.1	10	3.3	Pishan County
2015/7/3	22:37:05	37.6	77.9	10	3.1	Pishan County
2015/7/3	21:45:04	37.5	78.1	10	3.3	Pishan County
2015/7/3	21:41:32	37.4	78.1	10	3.4	Pishan County
2015/7/3	21:39:27	37.5	78.1	10	3.3	Pishan County
2015/7/3	20:56:21	37.5	78.1	10	3.4	Pishan County
2015/7/3	19:43:44	37.5	78.1	10	3.2	Pishan County
2015/7/3	19:21:30	37.6	77.9	10	3.2	Pishan County
2015/7/3	19:19:21	37.6	77.9	10	3.2	Pishan County
2015/7/3	18:59:04	37.6	78.1	10	3	Pishan County
2015/7/3	18:37:18	37.5	78.1	10	3.4	Pishan County
2015/7/3	17:18:36	37.6	77.9	5	3.4	Pishan County
2015/7/3	16:57:26	37.6	77.9	10	3.4	Pishan County
2015/7/3	15:27:21	37.6	78.1	9	3.4	Pishan County
2015/7/3	13:28:32	37.5	78	4	3.3	Pishan County
2015/7/3	13:20:32	37.5	78.2	8	3	Pishan County

Table 1 *continued*

Date	Origin time	Latitude	Longitude	Depth	Magnitude	Place
2015/7/3	13:06:29	37.5	78	10	3.6	Pishan County
2015/7/3	13:03:06	37.6	78.1	8	3	Pishan County
2015/7/3	12:43:49	37.5	78.2	8	3	Pishan County
2015/7/3	11:50:15	37.5	78.2	8	3.4	Pishan County
2015/7/3	11:50:12	37.5	78.2	8	3	Pishan County
2015/7/3	11:39:00	37.5	78.1	8	3	Pishan County
2015/7/3	11:17:18	37.5	78	5	3.2	Pishan County
2015/7/3	11:11:13	37.5	78.1	7	4.6	Pishan County
2015/7/3	11:10:06	37.6	77.7	21	3	Pishan County
2015/7/3	10:48:16	37.6	77.9	11	3	Pishan County
2015/7/3	10:37:27	37.5	77.9	10	4.2	Pishan County
2015/7/3	10:32:50	37.5	78.2	7	3.1	Pishan County
2015/7/3	10:28:34	37.6	77.8	10	3	Pishan County
2015/7/3	10:17:30	37.6	78.1	9	3.1	Pishan County
2015/7/3	10:13:44	37.5	78.1	10	3.1	Pishan County
2015/7/3	9:54:50	37.6	77.8	10	3	Pishan County
2015/7/3	9:44:45	37.4	78.2	10	4.5	Pishan County
2015/7/3	9:42:43	37.5	78	8	3	Pishan County
2015/7/3	9:34:53	37.6	77.9	9	3.6	Pishan County
2015/7/3	9:31:24	37.5	78	10	4.1	Pishan County
2015/7/3	9:29:54	37.5	78	7	3.2	Pishan County
2015/7/3	9:27:25	37.5	78.1	8	3.4	Pishan County
2015/7/3	9:25:12	37.5	77.8	9	4	Pishan County
2015/7/3	9:22:53	37.6	77.8	10	3.9	Pishan County
2015/7/3	9:20:05	37.1	78.2	9	3.2	Pishan County
2015/7/3	9:19:17	37.5	77.8	11	3.7	Pishan County
2015/7/3	9:13:17	37.6	77.9	8	4.6	Pishan County
2015/7/3	9:07:46	37.6	78.2	10	6.5	Pishan County

3.3. Location Vectors of Wenchuan Sequence

The Pishan earthquake occurred to the northwest of the array, and the location vectors showed an abnormal distribution. To investigate earthquakes originating from other directions, over 70 events from the Wenchuan sequence that occurred from May 12 to August 31, 2008 are investigated (the magnitude 8.9 Wenchuan earthquake resulted in thousands of fatalities); this catalog was also supplied by the CENC. The location vectors of the Wenchuan sequence are shown in Fig. 4b (the symbols in the diagram have the same meaning as in Fig. 4a). As shown in this figure, the observation values are all larger than the theoretical values, indicating systematic error.

The difference between the errors of the Pishan and Wenchuan earthquakes is that the observed values are all smaller than the theoretical values for the Pishan earthquakes, whereas the converse is true for the Wenchuan earthquake. A similarity is that the location vectors of the Wenchuan earthquake point in the same direction as those of the Pishan earthquake, i.e., 300°.

3.4. Location Vectors of Other Earthquakes

According to Harris (1990), Walck and Chael (1991), and Steck and Prothero (1993), lower values of SNR mean the results will be dispersed. Choosing events with magnitudes > 5.5 means that the SNR will be high and, therefore, location results will be more reliable. To evaluate the error distribution in the slowness domain, we collect data for 171 earthquakes (Fig. 5a) with magnitude > 5.5 from different back-azimuths and distances. For the teleseismic events, data from the catalog of the National Earthquake Information Center are taken as theoretical values. For the regional and local events, data from the catalog of the CENC are taken as theoretical values.

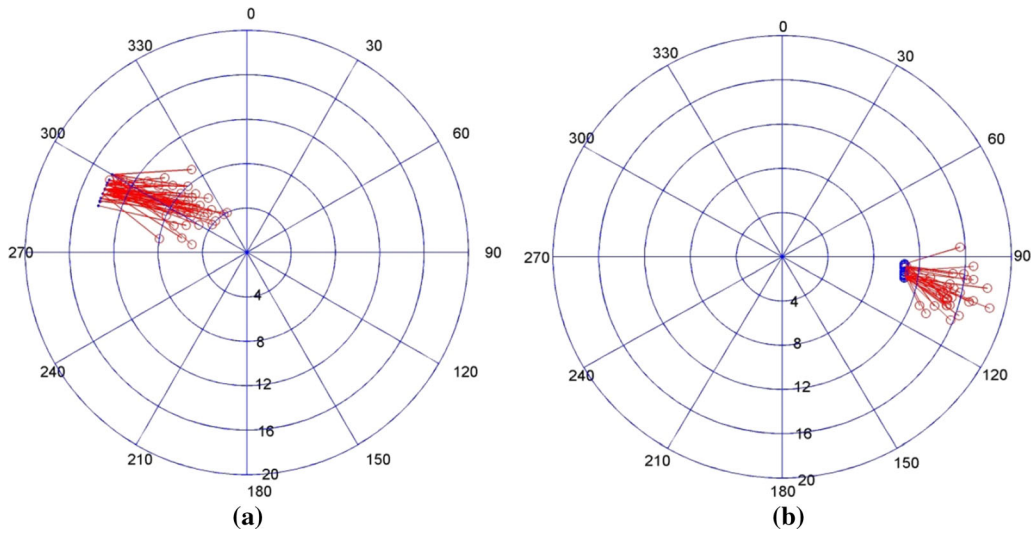

Figure 4
a Location error vectors of Pishan earthquake; red lines indicate theoretical values. Center of the diagram represents the Hotan array. The back-azimuth can be read clockwise from north (one tick every 30°), and the slowness in radial direction (one tick every 4 s/°). **b** Location error vectors of Wenchuan earthquake; the meaning of the symbols is the same as in **a**

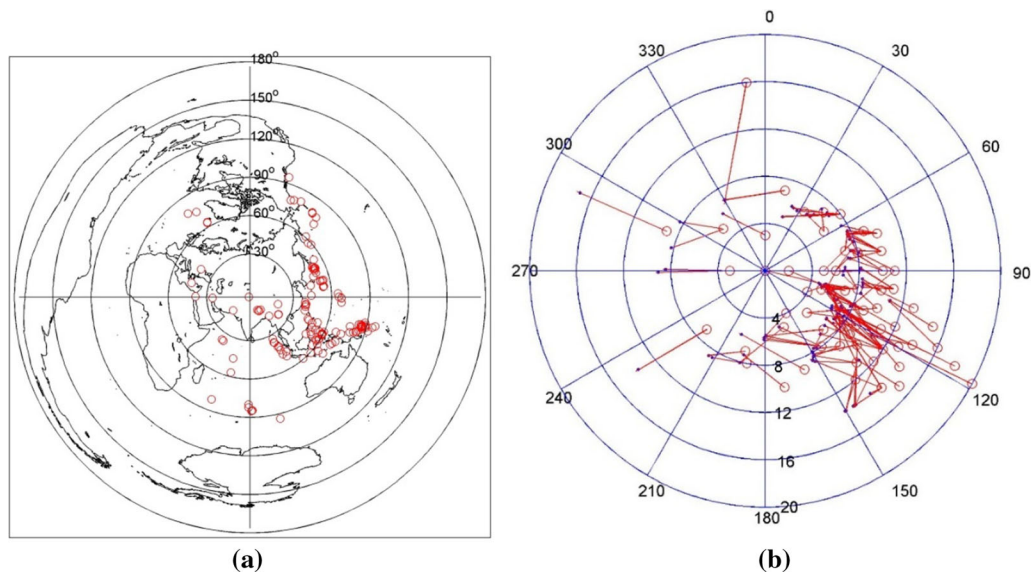

Figure 5
a Events used in the calculation of the locations and **b** error distribution of the events in all directions for the Hotan array. Circles represent calculated results; lines point to theoretical values

Most errors in the entire slowness domain point to the northwest, except in a few places (Fig. 5b).

The back-azimuth errors relative to the great circle back-azimuth change approximately as a cosine function (Fig. 6). The back-azimuth errors between 100° and 300° are negative, while the others are positive. This indicates that the back-azimuth errors of earthquakes coming from the south are

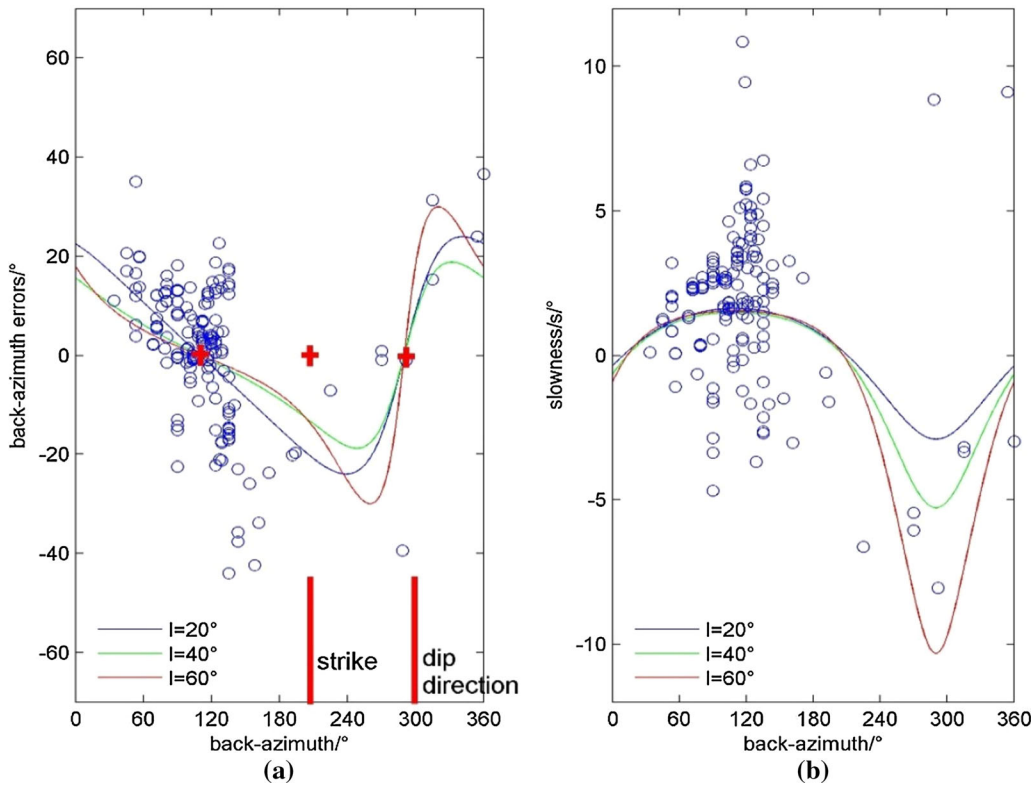

Figure 6
Observed back-azimuth and slowness errors as a function of the great circle back-azimuth and theoretical error curves when the angle of incidence is in the range of 20–60°

negative, whereas the back-azimuth errors of earthquakes coming from the north are positive. The slowness errors relative to the great circle back-azimuth also change approximately as a cosine function. At a back-azimuth of about 120°, the slowness errors can be either positive or negative and the scatter is large. Between 160° and 360°, the errors are negative, whereas the others are positive. These results mean that the slowness errors are negative when earthquakes come from the west and positive when earthquakes come from the east. As suggested by Niazi (1966), the error distribution in the Hotan array could be related to a dipping layer below the array. According to Niazi (1966), in the figure where the back-azimuth errors change together with the great circle back-azimuth, the point at which the sign of the back-azimuth errors change from negative to positive represents the dip direction, while the crossing point of the two points where the sign changes represents the strike. As shown in Fig. 6, the dip direction is therefore about 300° and the strike is about 210°.

3.5. *Estimation of Dip Angle of Dipping Layer*

The strike and dip directions are determined based simply on the above analysis. To determine the dip angle, the formulas given by Niazi (1966) are employed, from which it is possible to obtain theoretically the error curves for events with angles of incidence of 20–60° (Fig. 7). Based on comparison of the theoretical and observation error curves, it is concluded that the shapes of the theoretical error curves are similar to the observation error curves; For example, the back-azimuth at which the maximum observation back-azimuth errors appear is about 90° apart from the theoretical one, and the back-azimuth

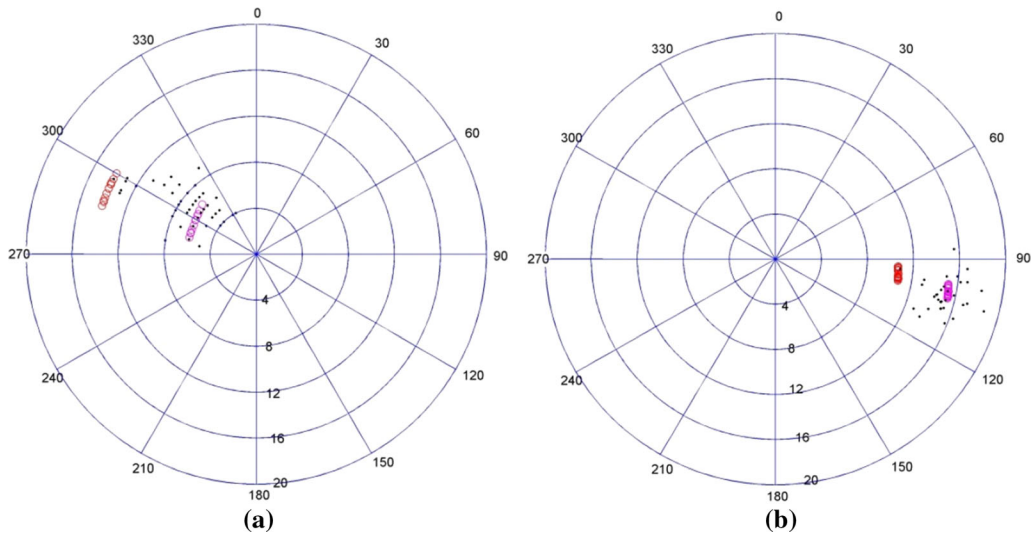

Figure 7
a Calculation values with dipping layer for the Pishan earthquake. Red circles represent theoretical values, pink circles represent calculation values with the dipping layer, and black dots represent observation values. **b** Calculation values with dipping layer for the Wenchuan earthquake; the meaning of the symbols is the same as in **a**

at which the maximum observation slowness errors appear is consistent with the theoretical one.

3.6. Evaluation of Dipping Layer Model

Three datasets are used to evaluate the dipping layer model. The grid search method is adopted to calculate the parameters of the dipping layer. Based on the research described above, the strike interval is selected as 190–230° and the dip direction interval as 40–50°. According to Chen and Chen (2003), the mean velocities of the upper, middle, and lower crust are 5.6, 6.26, and 6.76 km/s, respectively; the mean velocity of P waves is 8.11 km/s. Therefore, the velocity contrast interval of 0.6–0.9 is chosen. These parameter combinations are used to calculate the predicted values. The best combination is considered to be the one for which the predicted values differ least from the observed values. Thus, the best combination of parameters constitutes the dipping layer model.

For the Pishan sequence, the results of this study indicate that the strike, dip angle, and velocity contrast are 210°, 45° and 0.89, respectively, which could decrease the standard errors to 10.9° and 2.06 s/° from 14.6° and 6.4 s/°, respectively (Fig. 7a). For the Wenchuan sequence, the results indicate that the strike, dip angle, and velocity contrast are 210°, 45°, and 0.678, respectively, which could decrease the standard errors to 4.62° and 1.15 s/° from 6.21° and 4.38 s/°, respectively (Fig. 7b). For the other 171 earthquakes, the results indicate that the strike, dip angle, and velocity contrast are 210°, 45° and 0.89, respectively, which could decrease the standard errors to 10.3° and 2.47 s/° from 14.4° and 2.66 s/°, respectively (Fig. 8). The random errors that appear after the structure correction show that the systematic characteristics are successfully removed (Figs. 7, 8). Only the Wenchuan earthquakes showed a different velocity contrast, possibly because of inhomogeneity of the features of the ray paths between Wenchuan and the Hotan array. The mean value of the two velocity contrasts (0.78) is adopted as the final result. Thus, the dipping layer model is assigned strike, dip angle, and velocity contrast of 210°, 45°, and 0.78, respectively.

This method is unable to determine the depth of the dipping layer. If the depth of the dipping layer is required, the performance for regional and local events and the velocity contrast must be analyzed. The distance between the Pishan earthquakes (depth:

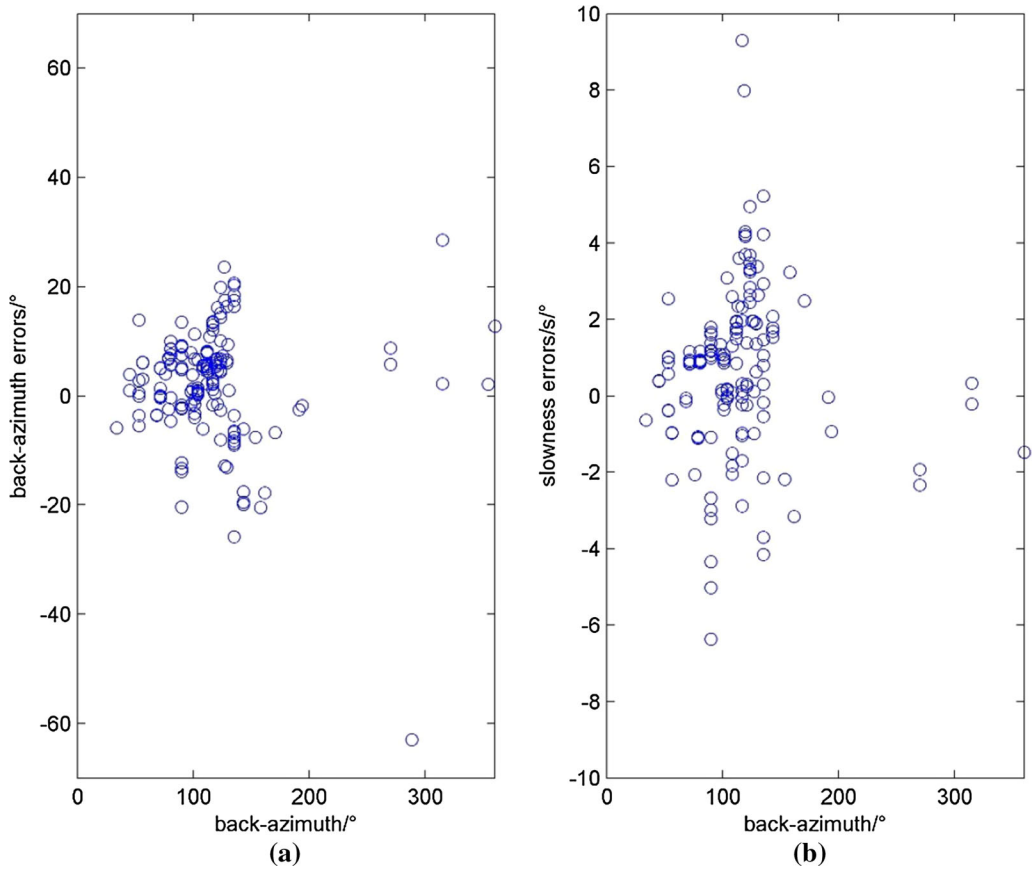

Figure 8
Errors after structure correction as a function of the great circle back-azimuth

10 km) and the Hotan array is about 0.8°, and the ray paths of the Pishan earthquakes do not penetrate to the Moho, according to Otsuka (1966). Systematic errors that appeared at the location of the Pishan earthquakes indicate that the dipping layer should lie in the crust. According to the results of Chen and Chen (2003), the velocity contrast of the upper and middle crust, middle and lower crust, and lower crust and upper mantle is 0.89, 0.93, and 0.83, respectively. The velocity contrast result from the Pishan sequence and the other 171 events is 0.89, which is in accordance with the results for the upper and middle crust. The velocity contrast result from the Wenchuan sequence is 0.678, which is not in accord with the results of Chen and Chen (2003). Three factors could cause this difference: the dipping Moho, as mentioned by both Gao et al. (2000) and Kao et al. (2001), the structure below the Wenchuan area, and inhomogeneity of the features of the ray paths between Wenchuan and the Hotan array. The derived results could be used to improve location accuracy.

4. Conclusions

This study establishes that systematic errors in the Hotan array could be related to a dipping layer below the array, for which the strike, dip, and velocity contrast are determined as 210°, 45°, and 0.78, respectively. Furthermore, it is found that the dipping layer lies within the crust, as revealed by the Pishan datasets.

After correction for this dipping layer, the location results of the Wenchuan and Pishan earthquakes

are improved by 25.5% for the back-azimuth and by 70.8% for slowness. For the other 171 earthquakes, the location results are improved by 28.5% for the back-azimuth and by 7.1% for slowness.

Acknowledgements

We thank the National Digital Seismic Network Data Backup Center of the Institute of Geophysics for supplying the waveform data. We offer our sincere thanks to the reviewers for their valuable comments that helped us improve the paper. We thank Sara J. Mason, M.Sc., from Liwen Bianji, Edanz Editing China (www.liwenbianji.cn/ac), for editing the English text of a draft of this manuscript.

Funding

Funding was provided by National Natural Science Foundation of China (CN) (Grant No. 41474114)

References

Aki, K., & Richards, P. G. (1980). *Quantitative seismology, theory and methods* (Vol. I and II). New York: W. H. Freeman.

Berteussen, K. A., Husebye, E. S., Mereu, R. F., & Ram, A. (1977). Quantitative assessment of the crust upper mantle heterogeneities beneath Gauribidanur seismic array in southern India. *Earth and Planetary Science Letters, 37,* 326–332.

Briden, J. C., Mereu, R. F., & Whitcombe, D. N. (1982). A teleseismic study of the West African craton margin in Senegal: P-wave slowness and azimuth anomalies. *Geophysical Journal of the Royal Astronomical Society, 71,* 793–808.

Capon, J. (1973). Signal processing and frequency wavenumber spectrum analysis for a large aperture seismic array. *Journal of Computational Physics, 13,* 1–59.

Chen, J. X., & Chen, J. L. (2003). The crustal structure and velocity feature from Ruoqiang-Altai seismic profile in Xinjiang Region. *Xinjiang Petroleum Geology, 26*(4), 498–501.

Chinnery, M. A., & Toksoz, M. N. (1967). P-wave velocities in the mantle below 700 km. *Bulletin of the Seismological Society of America, 57,* 199–226.

Cleary, J. R., Wright, C., & Muirhead, K. J. (1968). The effects of local structure upon Dt = dΔ measurements at the Warramunga seismic array. *Geophysical Journal of the Royal Astronomical Society, 16,* 21–29.

Dainty, A. M., & Battis, J. C. (1989). Variation of apparent azimuth of arrivals at a small aperture array in New England. *EOS, 70*(15), 400.

Davies, D., & Sheppard, R. M. (1972). Lateral heterogeneity in the earth's mantle. *Nature, 239,* 318–323.

Gao, R., Huang, D., Lu, D., Qian, G., Li, Y., Kuang, C., et al. (2000). Deep seismic reflection profile across the juncture zone between the Tarim basin and the West Kunlun Mountains. *Chinese Science Bulletin, 45,* 2281–2286.

Granet, M. (1986). A teleseismic study of the Upper Rhinegraben area: Array mislocation diagram and 3-D velocity inversion. *Journal Geophysical Research, 59,* 119–128.

Greenfield, R. J., & Sheppard, R. M. (1969). The Moho depth variations under the LASA and their effect on dT = dΔ measurements. *Bulletin of the Seismological Society of America, 59,* 409–420.

Harjes, H. P., & Henger, M. (1973). Array-seismologie. *Zeitschrift für Geophysik, 39,* 865–905.

Harris, D. B. (1990). Comparison of the direction estimation performance of high-frequency seismic arrays and three-component stations. *Bulletin of the Seismological Society of America, 80,* 1951–1968.

Hearty, D. J., Mereu, R. F., & Wright, C. (1977). Lateral variations in upper crustal structure below the La Malbaie area from slowness, azimuth, and traveltime measurements of teleseisms. *Canadian Journal of Earth Sciences, 14,* 2284–2293.

Kanasewich, E. R., Ellis, R. M., Chapman, C. H., & Gutowski, P. R. (1972). Teleseismic array evidence of inhomogeneities in the lower antle and the origin of the Hawaiian Islands. *Nature*, *239*, 99.

Kanasewich, E. R., Ellis, R. M., Chapman, C. H., & Gutowski, P. R. (1973). Seismic array evidence of a core boundary source for the Hawaiian linear volcanic chain. *Journal Geophysical Research, 78,* 1361–1371.

Kao, H., Gao, R., Rau, R. J., Shi, D., Chen, R. Y., Guan, Y., et al. (2001). Seismic image of the Tarim basin and its collision with Tibet. *Geology, 29*(7), 575–578.

Koch, K., & Kradolfer, U. (1999). Determination of mislocation vectors to evaluate bias at GSETT-3 primary stations. *Journal of Seismology,* **3,**139–151. *Bulletin of the Seismological Society of America, 87,* 1576–1597.

Lin, C. H., & Roecker, S. W. (1996). P-wave back azimuth anomalies observed by a small-aperture seismic array at Pinyon Flat, Southern California: Implication for structure and source location. *Bulletin of the Seismological Society of America, 86,* 470–476.

Niazi, M. (1966). Corrections to apparent azimuths and travel-time gradients for a dipping Mohorovicic discontinuity. *Bulletin of the Seismological Society of America, 56,* 491–509.

Niazi, M., & Anderson, R. F. (1965). Upper mantle structure of western North America from apparent velocities of P-waves. *Journal Geophysical Research, 70,* 4633–4640.

Otsuka, M. (1966). Azimuth and slowness anomalies of seismic waves measured on the Central California seismographic array. Part II. Interpretation. *Bulletin of the Seismological Society of America, 66,* 655–675.

Powell, C. (1975). Evidence for mantle heterogeneity from two large seismic arrays. *Nature, 254,* 40–42.

Ram, A., & Yadav, L. (1984). Structural corrections for slowness and azimuth of seismic signals arriving at Gauribidanur array. *Bulletin of the Seismological Society of America, 74,* 97–105.

Sengupta, M. K., & Julian, B. R. (1974). Mantle velocity and its regional variation. *EOS, 55,* 350.

Sheppard, R. M. (1967). *Values of LASA time station residuals, velocity and azimuth errors*. Technical Note, 1967-44, M.I.T. Lincoln Laboratory, Cambridge, Massachusetts.

Steck, L. K., & Prothero, W. A. (1993). Observations of direct P-wave slowness and azimuth anomalies for teleseisms recorded in Long Valley caldera, California. *Bulletin of the Seismological Society of America*, *83*, 1391–1419.

Walck, J. M., & Chael, E. P. (1991). Optimal back azimuth estimation for three-component recording of regional seismic events. *Bulletin of the Seismological Society of America, 81,* 643–666.

Walck, M. C., & Minster, J. B. (1982). Relative array analysis of upper mantle lateral velocity variations in southern California. *Journal Geophysical Research, 87,* 1754–1772.

Weichert, D. H. (1972). Anomalous azimuths of P: Evidence for lateral variations in the deep mantle. *Earth and Planetary Science Letters, 17,* 181–188.

Wright, C., Cleary, J. R., & Muirhead, K. J. (1974). The effects of local structure and the adjacent upper mantle on short period P-wave arrivals recorded at Warramunga seismic array. *Geophysical Journal of the Royal Astronomical Society, 36,* 295–319.

(Received August 27, 2018, revised July 9, 2019, accepted July 23, 2019, Published online August 7, 2019)